JACS
JOURNAL OF THE AMERICAN CHEMICAL SOCIETY
Article
pubs.acs.org/JACS

Unusual Stability of Acetonitrile-Based Superconcentrated Electrolytes for Fast-Charging Lithium-Ion Batteries

Yuki Yamada,[†,‡] Keizo Furukawa,[†] Keitaro Sodeyama,[‡,§] Keisuke Kikuchi,[†] Makoto Yaegashi,[†] Yoshitaka Tateyama,[‡,§,∥] and Atsuo Yamada*[,†,‡]

[†]Department of Chemical System Engineering, The University of Tokyo, Bunkyo-ku, Tokyo 113-8656, Japan

[‡]Elements Strategy Initiative for Catalysts & Batteries (ESICB), Kyoto University, Nishikyo-ku, Kyoto 615-8245, Japan

[§]International Center for Materials Nanoarchitectonics (MANA), National Institute for Materials Science (NIMS), Tsukuba, Ibaraki 305-0044, Japan

[∥]PRESTO, Japan Science and Technology Agency (JST), Kawaguchi, Saitama 333-0012, Japan

Supporting Information

ABSTRACT: The development of a stable, functional electrolyte is urgently required for fast-charging and high-voltage lithium-ion batteries as well as next-generation advanced batteries (e.g., Li−O_2 systems). Acetonitrile (AN) solutions are one of the most promising electrolytes with remarkably high chemical and oxidative stability as well as high ionic conductivity, but its low stability against reduction is a critical problem that hinders its extensive applications. Herein, we report enhanced reductive stability of a superconcentrated AN solution (>4 mol dm^{-3}). Applying it to a battery electrolyte, we demonstrate, for the first time, reversible lithium intercalation into a graphite electrode in a reduction-vulnerable AN solvent. Moreover, the reaction kinetics is much faster than in a currently used commercial electrolyte. First-principle calculations combined with spectroscopic analyses reveal that the peculiar reductive stability arises from modified frontier orbital characters unique to such superconcentrated solutions, in which all solvents and anions coordinate to Li^+ cations to form a fluid polymeric network of anions and Li^+ cations.

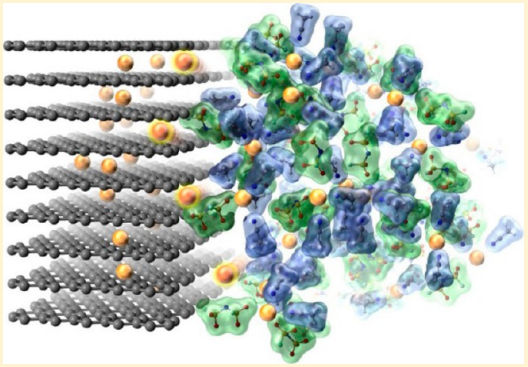

INTRODUCTION

With growing public concern about environmental and energy issues, considerable effort has been devoted to the development of cutting-edge electrochemical energy-storage technologies such as high-voltage and fast-charging lithium-ion batteries as well as next-generation lithium−oxygen batteries.[1−4] A key material in such advanced batteries is a stable, functional electrolyte that allows for reversible and rapid positive/negative electrode reactions without suffering from severe oxidative/reductive decompositions. In particular, an oxidation-tolerant electrolyte is primarily required to meet the recent remarkable progress and diversification of positive-electrode materials for high-voltage advanced batteries.

Acetonitrile (AN) is one of the most oxidation-tolerant organic solvents. In addition, due to its high dielectric constant,[5] AN can easily dissolve electrolyte salts to exhibit considerably high ionic conductivity. Because of these attractive features, AN solutions are a promising electrolyte for various electrochemical devices.[6−9] Particularly, applying them to lithium-ion batteries will eliminate the conventional voltage limitation (∼4.2 V) based on the electrochemical window of currently used carbonate-based electrolytes to open the possibility of high-voltage operation with a 5 V-class positive electrode.[4,10] Furthermore, the excellent ionic transport property will possibly realize fast-charging lithium-ion batteries, which are urgently required for automobile applications.

Despite these remarkable advantages, AN has not found extensive application in batteries. This is primarily due to its crucially poor reductive stability. AN spontaneously reacts with lithium metal (i.e., a strong reducing agent), and thus, a lithium metal electrode does not work reversibly in AN electrolytes.[11] For the same reason, there is no report on reversible lithium intercalation into graphite in AN solutions, excluding AN from the candidate of electrolytes for lithium-ion batteries. Hence, overcoming the poor reductive stability of AN will bring about substantial progress in next-generation advanced batteries.

Recently, we and our collaborative group have found that the electrochemical nature of organic solutions drastically change over a certain threshold of superhigh lithium-salt concentrations (i.e., over ca. 3 mol dm^{-3}); lithium salt-superconcentrated solutions not only suppress dangerous dendritic lithium deposition,[12] but also allow for a graphite negative-electrode reaction in propylene carbonate or dimethyl sulfoxide solution without using ethylene carbonate (EC) solvents.[13,14] Furthermore, we have found unusual reaction kinetics in a

Received: December 25, 2013
Published: March 23, 2014

   dx.doi.org/10.1021/ja412807w | J. Am. Chem. Soc. 2014, 136, 5039−5046

superconcentrated ether electrolyte despite its high viscosity.[15] Although the origin of the peculiar electrochemical features was not clear, such previous results motivated us to focus on "salt-superconcentrating" strategy to overcome the poor reductive stability of AN solvent and create a high-voltage and high-rate battery electrolyte exceeding a commercial EC-based one.

Herein, we report unusual reductive stability of a superconcentrated AN electrolyte and its origin based on spectroscopic analyses and quantum mechanical density functional theory based molecular dynamics (DFT-MD) simulations. With retaining AN's inherent high oxidative stability, the superconcentrated AN solution overcomes AN's low stability against reduction to allow for reversible graphite negative electrode reaction. More importantly, the superconcentrated AN electrolyte allows for ultrafast lithium intercalation into graphite, even much faster than in a currently used commercial EC-based electrolyte.

EXPERIMENTAL SECTION

Materials. Lithium bis(trifluoromethanesulfonyl)amide (LiTFSA), AN, and commercial 1.0 mol dm^{-3} $LiPF_6$/EC:dimethyl carbonate (DMC) electrolyte were purchased from Kishida Chemical Co., Ltd. and lithium bis(fluorosulfonyl)amide (LiFSA) was provided by Nippon Shokubai Co., Ltd. The reagents were all lithium-battery grade and used without further purification. Solutions were prepared by adding a given amount of lithium salt to AN with mild heating and stirring in an Ar-filled glovebox. Natural graphite powders (mean particle size: 10 μm) were provided by SEC Carbon, Ltd. and used without any pretreatment. To prepare a natural graphite electrode, the natural graphite powders were well mixed with 10 wt % polyvinylidene difluoride (PVdF, Kureha Corporation) in *N*-methylpyrrolidone (NMP, Wako Pure Chemical Industries, Ltd.). The slurry was uniformly spread onto a copper current collector (10 μm thickness) with a 50 μm doctor blade and dried at 120 °C under vacuum overnight. The obtained sheets were punched out to form a 16 mmϕ disk electrode. The active material loading was 0.60−0.70 mg cm^{-2}.

Physicochemical Properties. The density and viscosity of the solutions were evaluated with DMA 35 (Anton Paar GmbH) and Lovis 2000 M (Anton Paar GmbH), respectively. The reactivity between LiTFSA solutions and lithium metal foil was observed at room temperature. The ionic conductivity was measured by ac impedance spectroscopy at 1 kHz (Solartron 147055BEC, Solartron Analytical) in a two-electrode cell with platinum plates facing each other. All the measurements were conducted under pure argon atmosphere.

Electrochemical Measurements. Cyclic voltammetry and linear sweep voltammetry were performed by VMP-3 (BioLogic) in a three-electrode cell with a nickel or platinum plate as a working electrode and lithium metal foil as reference and counter electrodes. The charge−discharge test of natural graphite electrode was conducted in a 2032-type coin cell with a lithium metal negative electrode and a glass fiber separator (Whatman GF/F, 420 μm thickness) by a charge−discharge unit (TOSCAT, Toyo System Co., Ltd., or HJ1001SD8, Hokuto Denko Corporation). The temperature was controlled at 25 °C. Charge−discharge current was set at the ones corresponding to C/20, C/10, C/5, C/2, 1C, 2C, and 5C without using a constant-voltage mode at both ends of charge and discharge. Here, *x*C rate corresponds to the applied current of 372*x* mA g^{-1} on the weight basis of natural graphite. Cutoff voltage was set at 0 − 2.5 V. All the electrochemical measurements were carried out under argon atmosphere.

Spectroscopic Characterization. Surface chemistry of the natural graphite electrode was studied by X-ray photoelectron spectroscopy (XPS) using PHI 5000 VersaProbe (ULVAC-PHI, Inc.) equipped with a monochromatized Al Kα X-ray source. The graphite/lithium cell after one-cycle charge−discharge measurement was disassembled in an Ar-filled glovebox, and the graphite electrode was washed with DMC to remove the residual electrolyte components. The washed graphite electrode was dried and transferred into the XPS chamber without exposure to air. For comparison, the graphite electrode just immersed in the electrolyte for 24 h was studied in the same way as a standard. The binding energy was calibrated by using C 1s peak from sp^2 hybridized carbon at 284.5 eV as a reference. The peaks were assigned based on previous reports.[16−20] Curve fitting of spectra was performed with Voigt function (i.e., Gaussian−Lorentzian function) after a Shirley-type background subtraction. The relative sensitivity factors used for quantitative analyses are 0.314 (C1s), 0.733 (O1s), 1.00 (F1s), 0.717 (S2p), and 0.499 (N1s). The coordination structure of solutions was studied by Raman spectroscopy using NRS-1000 (JASCO Corporation) with an exciting laser of 514 nm. To prevent any contamination from air, the solution was put into a quartz cell and tightly sealed in it in an Ar-filled glovebox. The laser was radiated through the quartz crystal window. Peak deconvolution of obtained spectra was performed with Voigt function.

Computational Details. Car−Parrinello type DFT-MD simulations were carried out using CPMD code.[21,22] The cubic supercell with a 15.74 Å linear dimension is used for both diluted and concentrated LiTFSA/AN solutions. A fictitious electric mass of 500 au and a time step of 4 au (0.10 fs) were chosen. The temperature was controlled using a Nosé thermostat[23,24] with a target temperature of 298 K. After 5 ps equilibration steps, statistical averages were computed from trajectories of at least 10 ps in length (see Supporting Information, Figure S1). The electronic wave function was quenched to the Born−Oppenheimer surface every about 1 ps to keep adiabaticity. The energy cutoff of the plane wave basis is set to 90 Ry. Goedecker-Teter-Hutter type norm-conserving pseudopotentials[25−27] for C, H, O, N, S, F, and Li were used.

RESULTS AND DISCUSSION

Physical Properties and Reductive Stability. Basic set of information such as LiTFSA:AN molar ratio, density, viscosity, and ionic conductivity is presented in Table 1. All LiTFSA/AN mixtures in this work are a transparent, colorless liquid at room temperature. A superconcentrated 4.2 mol dm^{-3} solution, with the AN/LiTFSA molar ratio of 1.9, shows acceptable ionic conductivity of ca. 10^{-3} S cm^{-1} despite its high viscosity. As a visible indicator of reductive stability, we studied the reactivity of lithium metal foil, a strong reducing agent, in LiTFSA/AN systems (Figure 1). The lithium metal foil is quite unstable in a dilute 1.0 mol dm^{-3} solution; the lithium metal foil was immediately dissolved to turn the solution yellow. Since the reductive stability of AN is quite poor, AN would be easily reduced by lithium metal to produce a highly toxic free cyanide, as follows:[11]

$$CH_3CN + 2Li \rightarrow CH_3^- + CN^- + 2Li^+$$

Therefore, the lithium metal electrode cannot work in a conventional dilute AN electrolyte, and AN solvent has never been applied for advanced batteries despite its various advantages. In a superconcentrated 4.2 mol dm^{-3} LiTFSA/AN solution, however, no visible change was observed both for the lithium metal foil and for the solution, indicating that the

Table 1. Physicochemical Properties of LiTFSA/AN Solutions at 30 °C

concentration (mol dm^{-3})[a]	molar ratio (AN/LiTFSA)	density (g cm^{-3})	viscosity (mPa s)	conductivity (mS cm^{-1})
1.0	16	0.963	0.746	38.0
3.0	3.5	1.313	9.029	10.3
4.2	1.9	1.515	138.3	0.98

[a]The molar concentration is defined as the molar amount of lithium salt divided by the volume of the "whole solution" (not solvent only) in accordance with IUPAC.[28]

dx.doi.org/10.1021/ja412807w | J. Am. Chem. Soc. 2014, 136, 5039−5046

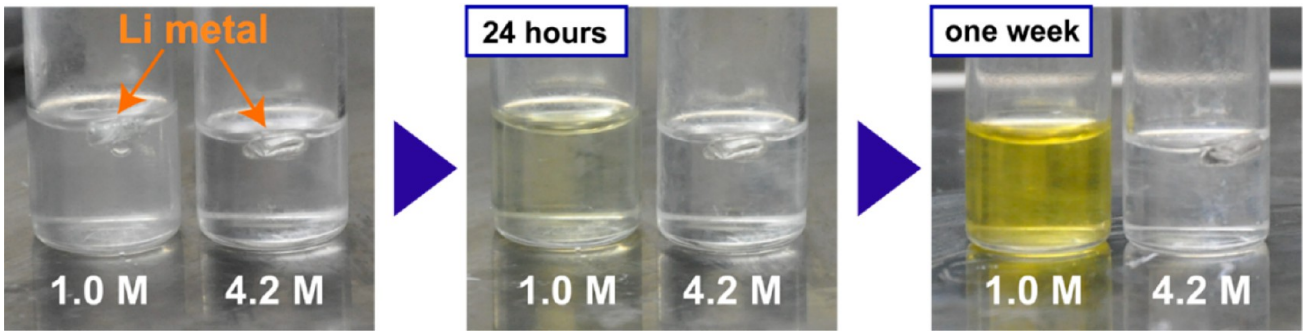

Figure 1. Reactivity of lithium metal foil and LiTFSA/AN solutions at 1.0 and 4.2 mol dm^{-3} concentrations at room temperature.

superconcentrated solution overcomes the inherent poor reductive stability of AN solvent to exhibit enhanced tolerance toward reduction. The unusual reductive stability was further proved by reversible lithium–metal deposition/dissolution reaction in 4.2 mol dm^{-3} LiTFSA/AN electrolyte (Figure S2). Although the reversibility is not good enough, this is the first to enable lithium metal to function as a reversible electrode in an AN-based electrolyte. Since the reaction is thoroughly irreversible in 3.0 mol dm^{-3} solution (Figure S3), the unusual reductive stability is unique to such superconcentrated solutions as 4.2 mol dm^{-3}. Note that oxidative stability is retained over 5 V vs Li/Li^+ reflecting AN's inherent high tolerance against oxidation (Figure S4).

Lithium Intercalation into Graphite. Having confirmed the enhanced reductive stability of the superconcentrated AN solution, we studied electrochemical lithium intercalation/deintercalation reaction at graphite electrode, which occurs at a quite low potential close to 0 V vs Li/Li^+. To ensure the practical validity of this superconcentrated electrolyte, the experiment is conducted under one of the most severe conditions; we used natural graphite without any surface treatment, which is quite inexpensive but difficult to obtain reversibility compared to widely used surface-treated natural graphite or synthetic graphite,[29] and also did not rely on any other techniques such as functional binders[30] or electrolyte additives[31−33] to facilitate reversible lithium intercalation. Figure 2 shows charge–discharge curves of a natural graphite/lithium metal coin cell using the 4.2 mol dm^{-3} LiTFSA/AN electrolyte. In the charge–discharge curves, several voltage plateaus appear in 0.05–0.25 V, which are characteristic of the sequential formation of several stage structures of lithium-graphite intercalation compound (Li-GIC).[34,35] The obtained reversible capacity was ca. 330 mAh g^{-1}, which is close to the theoretical capacity (372 mAh g^{-1}) based on fully lithiated LiC_6. These results clearly indicate the reversible lithium intercalation reaction at the natural graphite electrode. Without relying on any technique to facilitate lithium intercalation, we, for the first time, observed a reversible operation of a graphite negative electrode in an AN-based electrolyte. The successful lithium intercalation into graphite in one of the most reduction-vulnerable solvents validates our "salt-concentrating" strategy as a powerful and effective method of expanding the graphite negative-electrode reaction for a wide variety of organic solvents other than EC. To universalize this phenomenon, it is of critical significance to shed light on the mechanism of enhanced reductive stability in a superconcentrated solution.

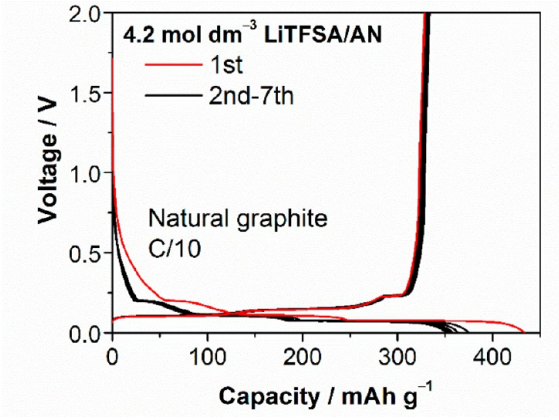

Figure 2. Charge–discharge curves of natural graphite/lithium metal cell with 4.2 mol dm^{-3} LiTFSA/AN electrolyte at C/10 rate.

Generally, a surface film (i.e., solid electrolyte interphase, SEI[36]) is a key to reversible lithium intercalation into graphite.[37,38] Therefore, we studied the surface atomic composition of the natural graphite electrode before and after a charge–discharge test in 4.2 mol dm^{-3} LiTFSA/AN electrolyte by XPS (Figure 3a,b). Unfortunately, we could not help avoiding a comparison with the SEI composition in a dilute 1.0 mol dm^{-3} electrolyte, because the experiment is highly dangerous due to the potential generation of free cyanide. Before a charge–discharge test (i.e., just immersed in 4.2 mol dm^{-3} LiTFSA/AN for 24 h, and washed with DMC), the major surface element was C from the natural graphite and partially from the PVdF binder. A small amount of F element should derive from the PVdF binder and the residual LiTFSA salt. The ratio of S and N elements, which are exclusively from LiTFSA or AN, is quite low compared to C element, suggesting that the residual electrolyte component is negligible after the wash with DMC. On the other hand, after one-cycle discharge and charge in the superconcentrated 4.2 mol dm^{-3} LiTFSA/AN electrolyte, the C element was remarkably decreased and the other elements, F, O, S, and N, became the main surface components. This indicates that the graphite electrode was covered with a surface film, whose composition is mainly F and O elements with non-negligible presence of S and N elements. From these results, the main component of the surface film in the superconcentrated system is reasonably regarded as decomposition products of a TFSA anion.

A detailed analysis on the surface film of the natural graphite cycled in 4.2 mol dm^{-3} LiTFSA/AN is shown in Figure 3c. The C1s spectrum displays five peaks representing graphite (sp^2), C–H/C–C (sp^3), C–O, CO_3/PVdF, and CF_3. It is characteristic of the present case that a large amount of CF_3 exists as one of the main chemical states of carbon element, in addition to

dx.doi.org/10.1021/ja412807w | J. Am. Chem. Soc. 2014, 136, 5039–5046

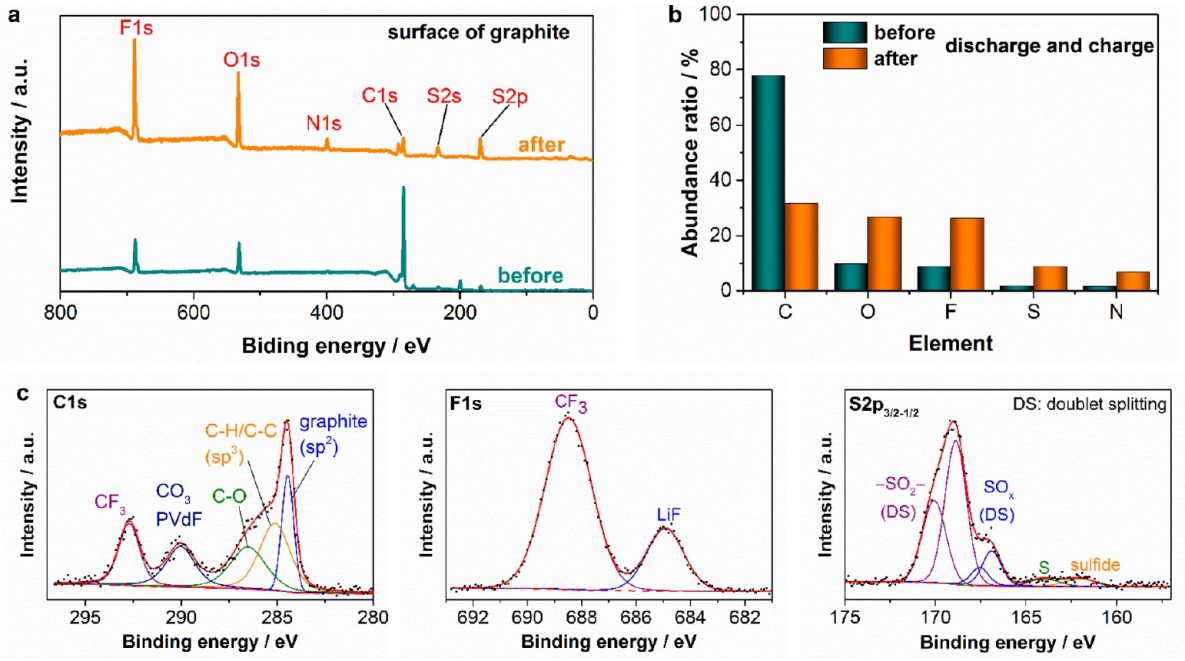

Figure 3. (a) Wide-scan XPS spectra for the natural graphite electrode before (just immersed in the electrolyte for 24 h) and after one-cycle charge and discharge in 4.2 mol dm^{-3} LiTFSA/AN electrolyte at C/10 rate. (b) Atomic ratio of C, O, F, S, and N on the surface of the natural graphite electrode obtained by the XPS spectra. (c) C 1s, F 1s, and S 2p spectra of the natural graphite electrode after one-cycle charge−discharge test (C/10 rate) in 4.2 mol dm^{-3} LiTFSA/AN electrolyte. Points and solid lines denote experimental spectra and fitting curves, respectively.

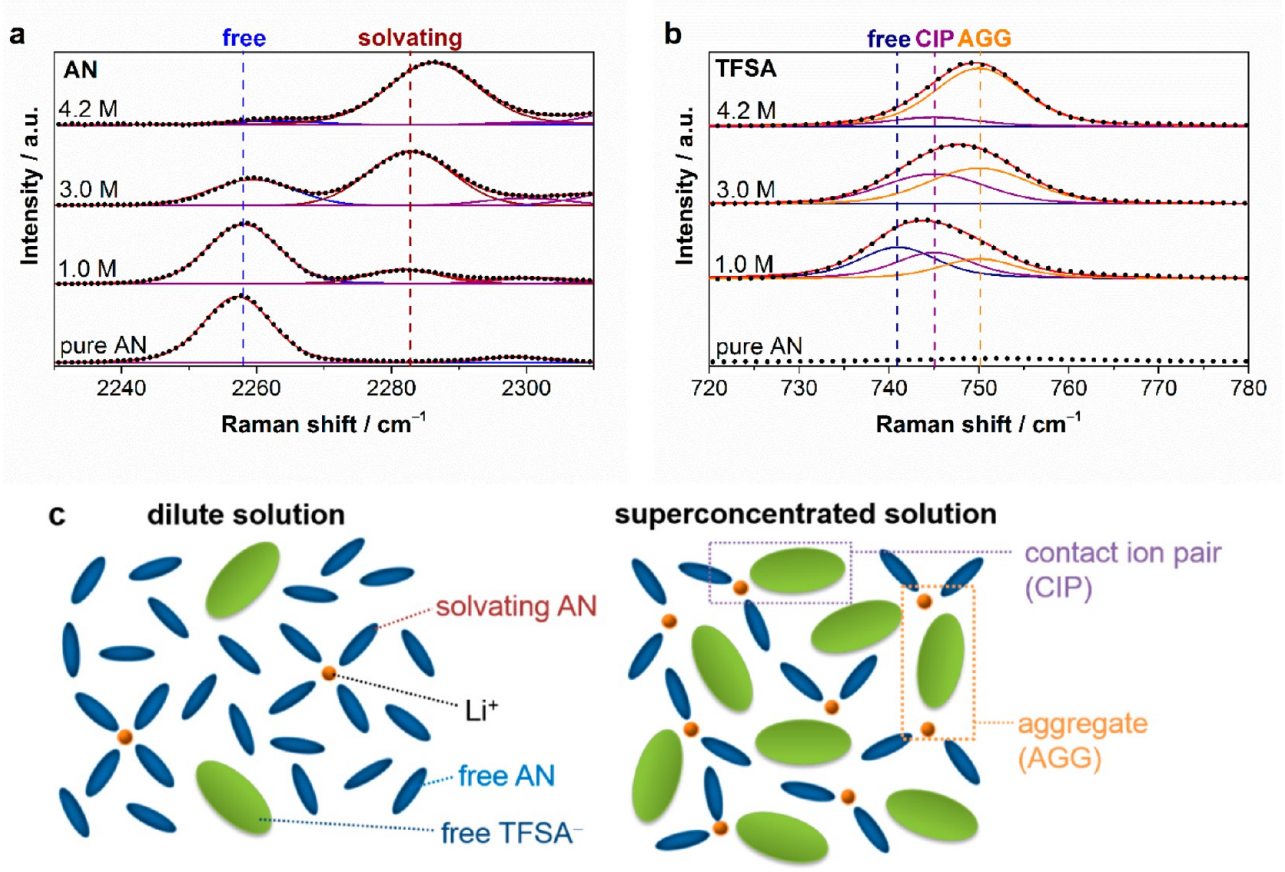

Figure 4. Raman spectra of LiTFSA/AN solutions in (a) 2230−2310 cm^{-1} (C≡N stretching mode of AN molecules) and (b) 720−780 cm^{-1} (S−N stretching, C−S stretching, and CF_3 bending mode of $TFSA^-$). Points and solid lines denote experimental spectra and fitting curves, respectively. (c) Representative environment of Li^+ in a conventional dilute solution (i.e., ∼1 mol dm^{-3}) and a salt-superconcentrated solution (i.e., 4.2 mol dm^{-3}).

dx.doi.org/10.1021/ja412807w | J. Am. Chem. Soc. 2014, 136, 5039−5046

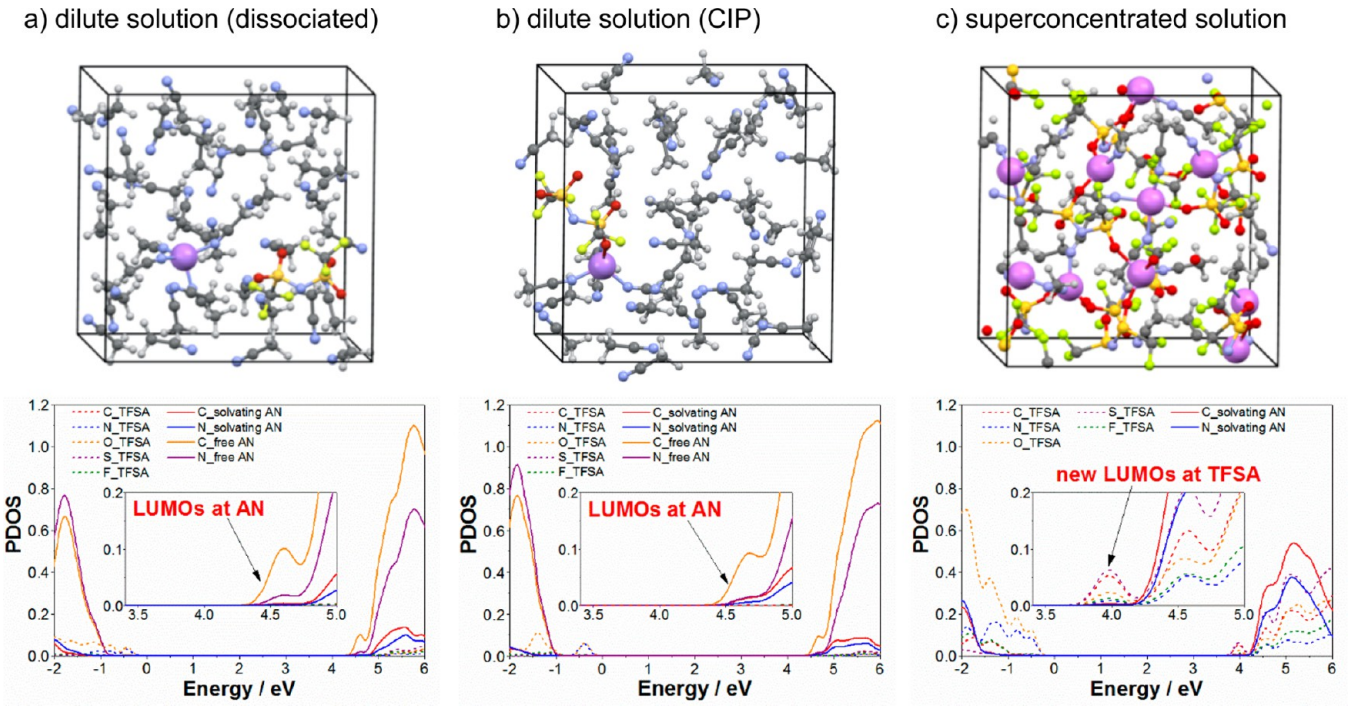

Figure 5. Supercells used and projected density of states (PDOS) obtained in quantum mechanical DFT-MD simulations on (a and b) dilute (1-LiTFSA/43-AN corresponding to 0.4 mol dm^{-3}) and (c) spuerconcentrated (10-LiTFSA/20-AN corresponding to 4.2 mol dm^{-3}) LiTFSA/AN solutions. The illustrated structures are the snapshots in equilibrium trajectories. For a dilute solution, both situations of LiTFSA salt (i.e., (a) full dissociation and (b) CIP) were considered. Atom color: Li, purple; C, dark gray; H, light gray; O, red; N, blue; S, yellow; F, green. Li atoms are highlighted in size. Insets in the PDOS profiles are magnified figures of the lowest energy-level edge of the conduction band.

those originating from graphite and its surface functional groups (e.g., sp^2, sp^3, and C−O). The CF_3 peak is also observed in the F 1s spectrum as the main chemical state of F element. The CF_3 component arises from decomposition products of a TFSA anion (and partially a residual LiTFSA salt). The F 1s spectrum also shows the presence of LiF, which should be formed by the decomposition of a LiTFSA salt. The S 2p spectrum, deconvoluted with spin−orbit split doublets (S $2p_{3/2}$ and S $2p_{1/2}$), shows the presence of $-SO_2-$ and SO_x with traces of S and sulfide. Since the only source of S is a TFSA anion in this system, all the species are from decomposition products of a TFSA anion. Less informative N 1s and O 1s spectra are presented in Figure S5, from which we could not identify their accurate chemical states due to the overlapping of several peaks at the almost same binding energy. Overall, there are plenty of evidence for the formation of a TFSA-derived surface film on the graphite electrode in the superconcentrated electrolyte. During the first lithium intercalation into graphite, the TFSA anion, instead of the AN solvent, is predominantly reduced to form a stable surface film, which corresponds to the irreversible capacity in the first cycle (Figure 2). Judging from the high Coulombic efficiency in the following cycle, the TFSA-derived surface film works as a protective layer to kinetically suppress further reductive decompositions of TFSA anions as well as AN solvents. In other words, due to the presence of the TFSA-derived protective surface film, the electrochemical window is kinetically widened to a cathodic direction in the superconcentrated AN solution. It is this situation that allows for reversible lithium intercalation/deintercalation at a graphite electrode by suppressing continuous reductive decompositions of AN solvents. This enhanced reductive stability, arising from modified film-forming ability, is unique to such a superconcentrated solution and contrary to the conventional belief that an AN-based electrolyte is never stable during lithium intercalation into graphite.

Solution Structure. To identify the solution structure providing the unusual reductive stability with a TFSA-derived surface film, Raman spectra were obtained for LiTFSA/AN solutions at various Li salt concentrations (Figure 4a,b). The Raman spectrum of pure AN in Figure 4a shows a C≡N stretching band (ν_2 mode) at 2258 cm^{-1} deriving from free AN molecules (i.e., without coordinating to Li^+).[39,40] At 1.0 mol dm^{-3} concentration, another ν_2 band appears at 2282 cm^{-1} arising from Li^+-solvating AN molecules.[39,40] In such dilute solutions, a stable solvation structure around Li^+ is reported to be 3- or 4-fold coordination (Figure 4c).[40,41] Further increasing the Li-salt concentration decreases free AN molecules and instead increases the Li^+-solvating AN molecules. At 4.2 mol dm^{-3} superhigh concentration, where unusual reductive stability was observed, there is only a peak for Li^+-solvating AN molecules, indicating that all the AN molecules coordinate to Li^+. Since the molar ratio of LiTFSA:AN is ca. 1:2 in 4.2 mol dm^{-3} LiTFSA/AN, Li^+ should have 2-fold AN coordination on average (Figure 4c). Further upshift of the ν_2 band at 4.2 mol dm^{-3} concentration indicates much stronger C≡N bond of AN, suggesting a peculiar coordination structure totally different from those in dilute solutions.

Turning to the vibration mode of $TFSA^-$ (i.e., S−N stretching, C−S stretching, and CF_3 bending) in Figure 4b, a deconvolution analysis shows that the Raman band consists of three peaks at 740, 745, and 750 cm^{-1}, arising from free anions, contact ion pairs (CIPs, $TFSA^-$ coordinating to a single Li^+ cation), and aggregates (AGGs, $TFSA^-$ coordinating to two or more Li^+ cations), respectively.[40] At 1.0 mol dm^{-3} concentration, the majority of $TFSA^-$ exists as free anions with small amount of CIPs and AGGs, due to the high salt dissociation

dx.doi.org/10.1021/ja412807w | J. Am. Chem. Soc. 2014, 136, 5039−5046

ability of AN arising from its high relative permittivity. With increasing Li-salt concentration, the free $TFSA^-$ anions decrease and disappear to form CIPs and AGGs over 3.0 mol dm^{-3} concentration. Finally, at 4.2 mol dm^{-3} superhigh concentration, almost all the $TFSA^-$ anions exist as AGGs with strong Coulombic interaction with multiple Li^+ cations. A series of spectroscopic analyses show that the structure of the salt-superconcentrated solution is characterized by a fluid polymeric network of mutually interacting $TFSA^-$ anions and Li^+ cations in the presence of two AN molecules solvating each Li^+. This peculiar structural feature is unique to such a superconcentrated solution, and should be a clue to its modified film-forming ability to provide unusual reductive stability.

Quantum Mechanical DFT-MD Simulation. To theoretically elucidate the origin of the unusual reductive stability with a TFSA-derived surface film, DFT-MD was applied to the dilute (1-LiTFSA/43-AN, 0.4 mol dm^{-3}) and superconcentrated (10-LiTFSA/20-AN, 4.2 mol dm^{-3}) LiTFSA/AN systems. Panels a and b of Figure 5 show snapshots and projected density of states (PDOS) of equilibrium trajectories of the dilute solution with a fully dissociated salt and CIP, respectively. Note that we examined PDOSs of several equilibrium geometries at different temperatures and confirmed the representative character (see Supporting Information, Figures S6 and S7). Here, we focused on conduction bands (i.e., unoccupied orbitals), which dominate the behavior of reduction reactions. In the dilute system with a fully dissociated salt (Figure 5a), the energy levels of Li^+-solvating or free AN molecules are lower than those of $TFSA^-$ anion at the lowest end of conduction bands; the lowest unoccupied molecular orbital (LUMO) is located at AN molecules. This indicates that AN molecules are predominantly reduced in a dilute LiTFSA/AN solution, which is consistent with the experimental result of continuous reductive decompositions of AN solvents in contact with lithium metal, a strong reduction reagent (Figure 1). The situation is the same when a simple ion pair (i.e., CIP) exists in the dilute solution (Figure 5b).

As for the superconcentrated solution (Figure 5c), the snapshot at an equilibrium trajectory shows a polymeric network of $TFSA^-$ anions and Li^+ cations: each $TFSA^-$ anion interacting with multiple Li^+ cations to form ion pairs (i.e., AGGs and partially CIPs), which is consistent with the results of Raman analyses (Figure 4) and totally different from those in dilute solutions. In the PDOS profile (Figure 5c), $TFSA^-$ anions provide new unoccupied states at the lowest energy in the conduction bands and the energy levels of $TFSA^-$ become lower than those of AN molecules; LUMO is located at $TFSA^-$ anions in the superconcentrated solution. The new unoccupied states are unique to such a superconcentrated solution with characteristic structural features of mutually networking $TFSA^-$ anions and Li^+ cations with a small amount of solvents. The localized LUMOs at the $TFSA^-$ anions suggest that $TFSA^-$ anions, rather than AN solvents, are predominantly reduced to form a TFSA-derived surface film on a graphite electrode in the superconcentrated electrolyte, which is fully consistent with the results of XPS analyses on the cycled graphite electrode (Figure 3). These quantum mechanical simulations with a realistic experimental salt concentration elucidate the peculiar frontier orbital characters in a salt-superconcentrated solution and account for the formation of a TFSA-derived surface film, which is the origin of the enhanced reductive stability to allow for reversible lithium intercalation into a graphite negative electrode.

Ultrafast Charging Character. It is well-known that overall charging rate of lithium-ion batteries largely depends on lithium intercalation kinetics at a graphite negative electrode, because the reaction potential of graphite is close to that of dangerous lithium metal and the polarization of lithium intercalation into graphite must be minimized to ensure a high level of safety.[42] In this regard, a practical problem lying in the superconcentrated 4.2 mol dm^{-3} LiTFSA/AN electrolyte is low reaction rate (Figure S8) arising from low ionic conductivity (0.98 mS cm^{-1}), high viscosity (138.3 mPa s), and presumably slow charge-transfer (Li^+ intercalation) process accompanied with decomplexation of AGGs and CIPs.

To remarkably improve the reaction kinetics, we next focus on a superconcentrated solution with another lithium salt, LiFSA, as a high-rate electrolyte, motivated by our recent report on a LiFSA-superconcentrated ether electrolyte.[15] LiFSA salt is characterized by weak interaction between Li^+ and FSA^- compared with that between Li^+ and $TFSA^-$ due to smaller electrostatic energy arising from the presence of large positive charge on the sulfur atoms as well as to smaller inductive energy arising from smaller polarizability of FSA^-.[43,44] The weaker Li^+-FSA^- binding energy as well as the smaller anion size results in high ionic conductivity and low viscosity in FSA-based ionic liquids,[43,44] which should also be true for salt-superconcentrated solutions with the formation of ion pairs (i.e., AGGs and CIPs). In addition, the weak Li^+-FSA^- binding energy should facilitate the decomplexation of AGGs and CIPs, presumably leading to fast Li^+ intercalation reaction. In fact, a superconcentrated 4.5 mol dm^{-3} LiFSA/AN solution has considerably high ionic conductivity (9.7 mS cm^{-1}) and relatively low viscosity (23.8 mPa s) (Table S1). As is the case with the LiTFSA/AN system, the superconcentrated LiFSA/AN electrolyte shows enhanced reductive stability to allow for reversible lithium intercalation into a graphite negative electrode (Figure S9).

Figure 6a shows lithium intercalation voltage curves of a natural graphite/lithium metal cell with superconcentrated 4.5 mol dm^{-3} LiFSA/AN and commercial EC-based electrolytes at various C-rates. Upon comparing the voltage curves in the two electrolytes, polarization (i.e., the downshift of voltage curve at higher C-rate) is considerably small in the superconcentrated electrolyte, indicating that lithium intercalation reaction is unusually fast and even far exceeds that in a currently used commercial EC-based electrolyte. Because of the small polarization arising from fast reaction kinetics, the superconcentrated 4.5 mol dm^{-3} LiFSA/AN electrolyte allows for massive lithium intercalation into a graphite electrode before the voltage reaches 0 V cutoff where dangerous lithium metal deposition occurs. Figure 6b shows C-rate dependence of the reversible capacity of a natural graphite/lithium metal half cell, where charge and discharge were conducted at the same C-rates. In a commercial EC-based electrolyte, the reversible capacity remarkably decreases with increasing rates, which is fully consistent with previous report in a similar experimental condition.[45,46] In contrast, the superconcentrated LiFSA/AN electrolyte exhibited much higher charging rate capability at all C-rates than not only a currently used commercial EC-based electrolyte but also a superconcentrated ether electrolyte we recently reported.[15]

We postulate that the ultrafast lithium intercalation should arise from several possible factors characteristic to the

dx.doi.org/10.1021/ja412807w | J. Am. Chem. Soc. 2014, 136, 5039−5046

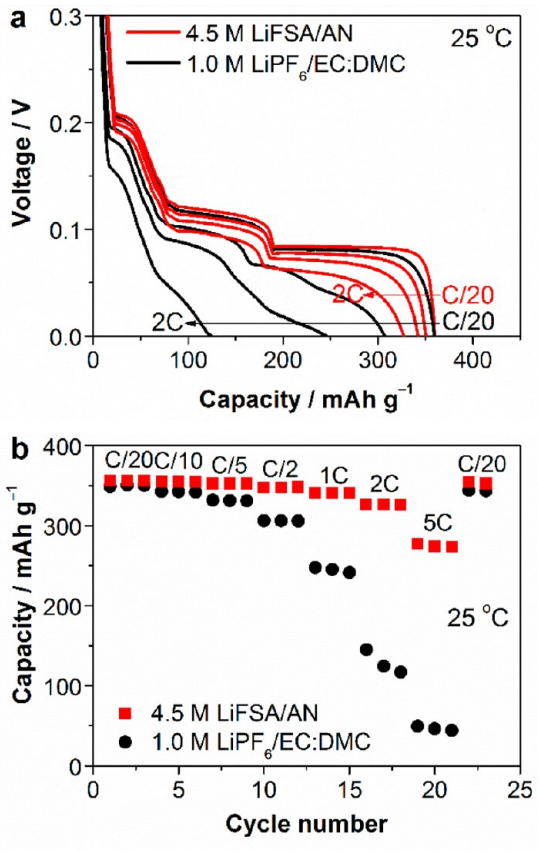

Figure 6. (a) Lithium intercalation voltage curves of a natural graphite/lithium metal half cell with superconcentrated 4.5 mol dm^{-3} LiFSA/AN and commercial 1.0 mol dm^{-3} $LiPF_6$/EC:DMC (1:1 by vol) electrolytes at various C-rates (C/20, C/2, 1C, and 2C) at 25 °C. (b) Reversible capacity of natural graphite in the two electrolytes at various C-rates and 25 °C. Charge and discharge were conducted at the same C-rate without using a constant-voltage mode at both ends of charge and discharge, and the charge (lithium deintercalation) capacity was plotted.

superconcentrated electrolyte: (i) high ionic transport properties (i.e., ionic conductivity and Li^+ transference number) presumably due to different Li^+-conduction mechanism from that in a dilute solution, (ii) high pre-exponential factor of lithium intercalation due to high interfacial Li^+ concentration, (iii) a good surface film facilitating lithium intercalation, and (iv) decomplexation kinetics of CIPs and AGGs different from desolvation. The detailed mechanism of ultrafast lithium intercalation, including charge-transfer mechanism at the interface and Li^+-conduction mechanism in the bulk electrolyte, is under investigation by both experimental and theoretical approaches, and will be reported elsewhere. Our finding of ultrafast lithium intercalation into graphite in a superconcentrated AN electrolyte will be an important breakthrough toward fast-charging lithium-ion batteries with expanding application to automobiles. In addition, the remarkable difference in the reaction kinetics depending on lithium salt species suggests the importance of anions in determining the physicochemical properties of superconcentrated electrolytes. The choice of anions as well as solvents will be a key in designing a better superconcentrated electrolyte with outstanding functionalities for advanced batteries.

CONCLUSIONS AND PERSPECTIVE

In summary, we have found enhanced reductive stability and ultrafast-charging character in a superconcentrated organic electrolyte for lithium-ion batteries. As an example, a superconcentrated AN solution overcomes the inherent low reductive stability of AN solvent to allow for reversible lithium intercalation into a graphite electrode. More importantly, the intercalation kinetics is much faster than in a currently used commercial electrolyte, and hence, the superconcentrated electrolyte can be an important breakthrough toward fast-charging lithium-ion batteries. The origin of enhanced reductive stability at superhigh salt concentrations was clarified by both experimental and theoretical approaches. A superconcentrated solution has a unique networking structure of Li^+ cations and $TFSA^-$ anions with Li^+-solvating AN solvents, which modifies frontier orbital characters in the solution; the LUMOs, which dominate the behavior of its reduction reaction, shift from AN solvents to $TFSA^-$ anions. Consequently, the $TFSA^-$ anions, instead of AN solvents, are predominantly reduced to form a TFSA-derived surface film on a graphite electrode during first lithium intercalation, which suppresses further decompositions of the electrolyte. The modified surface-film character, arising from the peculiar frontier orbitals, is the origin of the enhanced reductive stability of a superconcentrated solution that allows for reversible lithium intercalation into a graphite electrode without EC solvents. This work ensures the practical validity of superconcentrated organic solutions as a promising electrolyte for advanced batteries.

In the future, our superconcentrating strategy, expanding the graphite negative electrode reaction for a wide variety of organic solvents other than EC, will open a new research avenue in a functional electrolyte for advanced electrochemical technologies. In particular, the present breakthrough based on the superconcentrated AN electrolyte will be an important step toward high-voltage lithium-ion batteries utilizing graphite negative electrode and 5 V-class positive electrode, since the electrolyte allows for a reversible graphite negative-electrode reaction with retaining high oxidation potential over 5 V inherent to AN. Furthermore, the superconcentrated organic electrolyte can contribute to fast-charging lithium-ion batteries which are urgently required for automobile application. However, there are several problems to be overcome before consideration to practical applications. First, the Coulombic efficiency and cycle performance of a graphite electrode should be further improved. However, it should be noted that the present results are obtained under a severe condition; we used as-received natural graphite without any surface treatment,[29] functional binder,[30] or electrolyte additive.[31−33] Relying on these techniques facilitating reversible lithium intercalation will remarkably improve the Coulombic efficiency and cycle performance. Second, the corrosion of an aluminum current collector by a LiTFSA salt might be a problem. This side reaction will easily be suppressed by simple addition of a small amount of another salt such as $LiPF_6$.[2] Although it will be a long way to realize a superconcentrated electrolyte in practical application after resolving all above problems and also the issue of cost, we believe that the peculiar electrochemical feature and its detailed mechanism presented herein will be of great value not only in the development of next-generation advanced batteries but also in the fundamental research in electrochemistry and solution chemistry.

dx.doi.org/10.1021/ja412807w | J. Am. Chem. Soc. 2014, 136, 5039−5046

■ ASSOCIATED CONTENT

Supporting Information

Total energy profiles of DFT-MD simulation step, lithium metal deposition/dissolution, oxidative stability, N 1s and O 1s spectra, PDOS of different DFT-MD trajectories or different initial configuration convergence, rate-performance, physico-chemical properties of LiFSA/AN, and charge−discharge curves in LiFSA/AN. This material is available free of charge via the Internet at http://pubs.acs.org.

■ AUTHOR INFORMATION

Corresponding Author

yamada@chemsys.t.u-tokyo.ac.jp

Notes

The authors declare no competing financial interest.

■ ACKNOWLEDGMENTS

This work was supported by Advanced Low Carbon Technology Research and Development Program (ALCA) of JST and ESICB project of Ministry of Education, Culture, Sports, Science and Technology (MEXT), Japan. Y.T. and K.S. acknowledge KAKENHI 23340089 as well as the Strategic Programs for Innovative Research (SPIRE), MEXT and the Computational Materials Science Initiative (CMSI), Japan. The calculations in this work were carried out on the supercomputer centers of NIMS, ISSP and ITC (Oalkleaf-FX) in the University of Tokyo, as well as the K computer at the RIKEN AICS.

■ REFERENCES

(1) Bruce, P. G.; Freunberger, S. A.; Hardwick, L. J.; Tarascon, J.-M. *Nat. Mater.* **2012**, *11*, 19−29.
(2) Tarascon, J.-M.; Armand, M. *Nature* **2001**, *414*, 359−367.
(3) Armand, M.; Tarascon, J.-M. *Nature* **2008**, *451*, 652−657.
(4) Goodenough, J. B.; Kim, Y. *Chem. Mater.* **2010**, *22*, 587−603.
(5) *Organic Solvents: Physical Properties and Methods of Purification*, 4th ed.; Riddick. J. A., Bungh, W. B., Sakano, T. K., Eds.; Willey: New York, 1986.
(6) Mizuno, F.; Nakanishi, S.; Shirasawa, A.; Takechi, K.; Shiga, T.; Nishikoori, H.; Iba, H. *Electrochemistry* **2011**, *79*, 876−881.
(7) Peng, Z.; Freunberger, S. A.; Hardwick, L. J.; Chen, Y.; Giordani, V.; Bardé, F.; Novák, P.; Graham, D.; Tarascon, J.-M.; Bruce, P. G. *Angew. Chem.* **2011**, *123*, 6475−6479.
(8) Sarangapani, S.; Tilak, B. V.; Chen, C.-P. *J. Electrochem. Soc.* **1996**, *143*, 3791−3799.
(9) Hagfeldt, A.; Boschloo, G.; Sun, L.; Kloo, L.; Pettersson, H. *Chem. Rev.* **2010**, *110*, 6595−6663.
(10) Manthiram, A. *J. Phys. Chem. Lett.* **2011**, *2*, 176−184.
(11) Rupich, M. W.; Pitts, L.; Abraham, K. M. *J. Electrochem. Soc.* **1982**, *129*, 1857−1861.
(12) Jeong, S.-K.; Seo, H.-Y.; Kim, D.-H.; Han, H.-K.; Kim, J.-G.; Lee, Y. B.; Iriyama, Y.; Abe, T.; Ogumi, Z. *Electrochem. Commun.* **2008**, *10*, 635−638.
(13) Jeong, S.-K.; Inaba, M.; Iriyama, Y.; Abe, T.; Ogumi, Z. *Electrochem. Solid-State Lett.* **2003**, *6*, A13−A15.
(14) Yamada, Y.; Takazawa, Y.; Miyazaki, K.; Abe, T. *J. Phys. Chem. C* **2010**, *114*, 11680−11685.
(15) Yamada, Y.; Yaegashi, M.; Abe, T.; Yamada, A. *Chem. Commun.* **2013**, *49*, 11194−11196.
(16) Verma, P.; Maire, P.; Novák, P. *Electrochim. Acta* **2010**, *55*, 6332−6341.
(17) Leroy, S.; Martinez, H.; Dedryvère, R.; Lemordant, D.; Gonbeau, D. *Appl. Surf. Sci.* **2007**, *253*, 4895−4905.
(18) Diaz, J.; Paolicelli, G.; Ferrer, S.; Comin, F. *Phys. Rev. B* **1996**, *54*, 8064−8069.
(19) Leroy, S.; Blanchard, F.; Dedryvère, R.; Martinez, H.; Carré, B.; Lemordant, D.; Gonbeau, D. *Surf. Interface Anal.* **2005**, *37*, 773−781.
(20) Ensling, D.; Stjerndahl, M.; Nytén, A.; Gustafsson, T.; Thomas, J. O. *J. Mater. Chem.* **2009**, *19*, 82−88.
(21) Car, R.; Parrinello, M. *Phys. Rev. Lett.* **1985**, *55*, 2471−2474.
(22) CPMD, http://www.cpmd.org/, Copyright IBM Corp 1990−2008, Copyright MPI für Festkörperforschung Stuttgart 1997−2001 (accessed Feb 19, 2014).
(23) Nosé, S. *J. Chem. Phys.* **1984**, *81*, 511−519.
(24) Hoover, W. G. *Phys. Rev. A* **1985**, *31*, 1695−1697.
(25) Goedecker, S.; Teter, M.; Hutter, J. *Phys. Rev. B* **1996**, *54*, 1703−1710.
(26) Hartwigsen, C.; Goedecker, S.; Hutter, J. *Phys. Rev. B* **1998**, *58*, 3641−3662.
(27) Krack, M. *Theor. Chem. Acc.* **2005**, *114*, 145−152.
(28) IUPAC. *Quantities, Units and Symbols in Physical Chemistry*, 3 ed.: RSC Publishing: Cambridge, 2007.
(29) Wu, Y. P.; Jiang, C.; Wan, C.; Holze, R. *Solid State Ionics* **2003**, *156*, 283−290.
(30) Komaba, S.; Ozeki, T.; Okushi, K. *J. Power Sources* **2009**, *189*, 197−203.
(31) Wrodnigg, G. H.; Besenhard, J. O.; Winter, M. *J. Electrochem. Soc.* **1999**, *146*, 470−472.
(32) Aurbach, D.; Bamolsky, K.; Markovsky, B.; Gofer, Y.; Schmidt, M.; Heider, U. *Electrochim. Acta* **2002**, *47*, 1423−1439.
(33) Zhang, S. S. *J. Power Sources* **2006**, *162*, 1379−1394.
(34) Dahn, J. R. *Phys. Rev. B* **1991**, *44*, 9170−9177.
(35) Ohzuku, T.; Iwakoshi, Y.; Sawai, K. *J. Electrochem. Soc.* **1993**, *140*, 2490−2498.
(36) Peled, E. *J. Electrochem. Soc.* **1979**, *126*, 2047−2051.
(37) Aurbach, D. *J. Power Sources* **2000**, *89*, 206−218.
(38) Yazami, R. *Electrochim. Acta* **1999**, *45*, 87−97.
(39) Brouillette, D.; Irish, D. E.; Taylor, N. J.; Perron, G.; Odziemkowski, M.; Desnoyers, J. E. *Chem. Chem. Phys.* **2002**, *4*, 6063−6071.
(40) Seo, D. M.; Borodin, O.; Han, S.-D.; Boyle, P. D.; Henderson, W. A. *J. Electrochem. Soc.* **2012**, *159*, A1489−A1500.
(41) Seo, D. M.; Boyle, P. D.; Borodin, O.; Henderson, W. A. *RSC Adv.* **2012**, *2*, 8014−8019.
(42) Zaghib, K.; Goodenough, J. B.; Mauger, A.; Julien, C. *J. Power Sources* **2009**, *194*, 1021−1023.
(43) Borodin, O.; Gorecki, W.; Smith, G. D.; Armand, M. *J. Phys Chem. B* **2010**, *114*, 6786−6798.
(44) Tsuzuki, S.; Hayamizu, K.; Seki, S. *J. Phys. Chem. B* **2010**, *114*, 16329−16336.
(45) Sivakkumar, S. R.; Nerkar, J. Y.; Pandolfo, A. G. *Electrochim. Acta* **2010**, *55*, 3330−3335.
(46) Ding, F.; Xu, W.; Choi, D.; Wang, W.; Li, X.; Engelhard, M. H.; Chen, X.; Yang, Z.; Zhang, J.-G. *J. Mater. Chem.* **2012**, *22*, 12745−12751.